J Mater Sci: Mater Electron (2016) 27:11371–11378
DOI 10.1007/s10854-016-5262-2

Dielectric and photoluminescence properties of Nd and Ga codoped-$BaTiO_3$, prepared by sol–gel method

Marin Cernea[1] · Catalina Andreea Vasilescu[2,3] · Mihail Secu[1] · Gheorghe Aldica[1] · Adrian Surdu[2] · Paul Ganea[1]

Received: 14 April 2016 / Accepted: 27 June 2016 / Published online: 12 July 2016

Abstract Neodymium and gallium codoped barium titanate ($Ba_{1-x-y}Nd_xGa_yTiO_3$, x = 0.03, 0.05, 0.07, 0.1 and y = 0.03) were prepared by sol–gel method in order to investigate its dielectric and photoluminescence properties. The structure and morphology of $Ba_{1-x-y}Nd_xGa_yTiO_3$ powders calcined at 1100 °C and sintered ceramics by spark plasma sintering (SPS) technique were analyzed using X-ray diffraction and scanning electron microscope, respectively. The photoluminescence and dielectric properties of Nd doped $Ba_{0.97}Ga_{0.03}TiO_3$, (y = 0.03) as a function of Nd^{3+} concentration and sintering temperature were also investigated. The influence of Ga^{3+} and Nd^{3+} dopants on the crystalline phases, sintering process by SPS and macroscopic properties of $Ba_{1-x-y}Nd_xGa_yTiO_3$ ceramics was analyzed, as well as a weak hot emission from the 4F5/2 level. The sintered ceramics showed high dielectric constant and moderate dielectric losses. The highest value of the permittivity obtained for $Ba_{1-x-y}Nd_xGa_yTiO_3$ ceramics was $\varepsilon_r = 5890$ at room temperature, 1 kHz and x = y = 0.03. This study shown that Nd^{3+} decreases the density of the pellets, increases the dielectric losses and decreases the dielectric constant of $Ba_{0.97}Ga_{0.03}TiO_3$ ceramics. Therefore, the values of dielectric properties, at room temperature, of $BaTiO_3$ doped with 3 at.% Ga and ≤7 at.% Nd are higher than those of undoped $BaTiO_3$ ceramic.

✉ Catalina Andreea Vasilescu
catalina.a.stanciu@gmail.com

[1] National Institute of Materials Physics, P.O. Box MG-7, 077125 Magurele, Romania

[2] Politehnica University of Bucharest, 1-7 Gh. Polizu, 011061 Bucharest, Romania

[3] National Institute for Lasers, Plasma and Radiation Physics, P.O. Box MG54, 077125 Magurele, Romania

1 Introduction

Due to its ferroelectric properties, $BaTiO_3$ is widely studied for applications in optical devices, thermistors, tunable microwave devices and multilayer ceramic capacitors [1–8]. In order to improve the luminescent properties of the $BaTiO_3$, Fe^{2+} [9], Fe^{3+} [10], Pr^{3+} [11], Eu^{3+} [12], Er^{3+} [13], Yb^{3+} [14] ions have been used as dopants. La^{3+} [15], Nb^{5+} [16], Ru^{4+} [17] and Gd^{3+} [18] were used to improve the dielectric properties of barium titanate. Recent studies on neodymium doped barium titanate and gallium doped $BaTiO_3$ ceramics have shown that the Nd^{3+} and Ga^{3+} ions can modify the structure and dielectric properties of $BaTiO_3$ ceramic. The substitution of barium ions (Ba^{2+}) with neodymium (Nd^{3+}) [19–23] or gallium ions (Ga^{3+}) [24] on A-sites can induce A-site cation disorders and structural defects that influence the dielectric behavior of modified barium titanate ceramic. Many reports on Nd doped $BaTiO_3$ have been published, but only a few works about $BaTiO_3$ doped with Ga and, any articles about simultaneous doping of $BaTiO_3$ with Ga and Nd. In several studies, gallium appears as co-dopant along with: Y, Mg, Si, La, Mn, Zn [25–28].

Doping $BaTiO_3$ with Ga and Nd we expected to obtain materials with enhanced electric and optic properties knowing that Ga improves the dielectric properties of $BaTiO_3$ [25, 26, 28, 29] while Nd influences the photoluminescence properties of $BaTiO_3$ [22]. Gallium and neodymium have also influence on the photoluminescence and electrical properties of $BaTiO_3$ [19, 21, 30]. We have chosen to add 3 at.% Ga at $BaTiO_3$ because it is proved that this concentration is in the solubility domain of Ga in $BaTiO_3$ [25, 28, 30] and 10 at.% Nd is also in the solubility limits of Nd in $BaTiO_3$ [19].

Undoped and Nd or Ga doped $BaTiO_3$ powders were prepared by various methods as: conventional solid state

reactions [19, 30], sol–gel route [22], hydrothermal synthesis [20, 21, 23], etc. As sintering methods for perovskite powders were used: the conventional method [21, 37], microwave method [31, 32], spark plasma sintering (SPS) method [33–35], etc.

Compared with traditional sintering procedure, SPS enables to sinter compact powders to a higher density at a relatively lower temperature in a shorter sintering period [33]. SPS has an advantage of suppressing exaggerated grain growth over conventional sintering. SPS equipment allows to obtain very high heating rates, due to the optimal thermal transfer existing between the heating element (the graphite die) and the sample, and the low thermal inertia of the graphite die itself. For example, Chen et al. [34], sintered $BaTiO_3$ ceramic at a temperature of about 1300 °C, 1 h or longer, resulting ceramics with grain size at the micrometer level. Luan et al. [35], prepared high density, fine-grained $BaTiO_3$ ceramics at the much lower temperature of 900 °C and at short sintering periods of some minutes by the SPS method. It is concluded that the short sintering period is advantageous in suppressing exaggerated grain growth.

Sintering materials by direct microwave heating shows various fundamental problems versus SPS sintering. Firstly, most of the research on material processing by microwaves is based on conventional low-frequency (2.45 GHz) microwave applicators; however, such applicators do not couple microwave power efficiently to many materials at room temperature and poor microwave absorption characteristics make initial heating difficult [36]. Thermal instabilities may occur, which can lead to the temperature non-uniformities that may cause non-uniform properties and cracking [36]. Finally, in a microwave heating, the direction of heating is from inside to outside of the powder compact resulting in higher temperature of the sample core than the surface. The former mode of heating results in poor microstructural characteristics of the surface [37–39].

In this work, we used gallium and neodymium as co-dopants for $BaTiO_3$. We present the preparation of $BaTiO_3$ doped with Nd^{3+} and Ga^{3+} powders via the sol–gel method and sintering ceramics by spark plasma technique. Structural, microstructural, dielectric and photoluminescence characteristics of as-prepared Nd and Ga doped $BaTiO_3$ materials are also presented in this paper.

2 Materials and methods

$Ba_{1-x-y}Nd_xGa_yTiO_3$, x = 0.03, 0.05, 0.07 and 0.1 and, y = 0.03 powders were prepared by sol–gel method starting from barium acetate ($(CH_3COO)_2Ba$, 99 %, Aldrich), titanium (IV) isopropoxide, ($Ti[OCH(CH_3)_2]_4$, Aldrich), gallium nitrate $Ga(NO_3)_3{\cdot}xH_2O$ and neodymium(III) acetate hydrate $(CH_3CO_2)_3Nd{\cdot}xH_2O$. Acetic acid (≥99.7 %, Aldrich) was used as solvent. The mixtures of barium, neodymium and gallium acetic solutions were added drop wise to the titanium isopropoxide solution in isopropanol (titanium(IV) isopropoxide was mixed with isopropanol in a ratio of 1:10) to produce a Ba–Nd–Ga–Ti complex solutions (sols). The sols were stabilized by adding acetylacetone ($C_5H_8O_2$, Aldrich). The as-obtained sols were maintained under continuous stirring at 75 °C, for 4 h, in order to obtain the gels. After drying the gels at ~100 °C, the resulting powders were treated at different temperatures for preparation of mono-phased powders. Perovskite $BaTiO_3$ cubic monophase was obtained after calcinations of gel-powders at 1100 °C for 3 h in air.

The as-obtained powders of $Ba_{1-x-y}Nd_xGa_yTiO_3$ were sintered as discs having thicknesses of about 2 mm and diameters of 20 mm by SPS technique using a commercial SPS machine (FCT Systeme GmbH—HP D 5, Germany). In order to prepare a ceramic disc by SPS, the powder was poured into a graphite die and uniaxial pressed at 16 MPa using a hydraulic press. Then, the graphite die with pressed powder were introduced into the SPS equipment, where a pressure of up to 63 MPa was applied, in vacuum of about 35 Pa. In the SPS equipment, a current pulse pattern was applied. The shape of the waveform was not square, but consisted of several spikes (pulses) separated by a current-free interval. Each pulse had the same period, of about 3×10^{-3} s. In the current work, a pattern of 12:2 on:off pulses was applied. The total time of one sequence (cycle) was about 0.04 s. The operating parameters, namely voltage and the peak current, were below 5 V and 1600 A, respectively. No sintering aid was added. The temperature was monitored with a pyrometer placed at 0.4 cm above the sample, in the punch and through an axial hole. The samples with various x values were sintered at different temperatures in order to achieve an advanced powder densification for each composition, as is shown in Table 1.

Figure 1 shows the variation of displacement (d), temperature (T), and mechanical pressure (P), as a function of time, during the SPS processing of the sample, the $Ba_{1-x-y}Nd_xGa_yTiO_3$ powder, were x = 0.1 and y = 0.03.

For this composition, the heating rate was 100 °C/min, up to 1210 °C. Densification begins at 1200 °C. At this temperature, a supplementary pressure was applied, up to 80 MPa (Fig. 1). No further densification could be achieved by increasing this temperature.

After SPS processing, the sintered pellets were contaminated with carbon from the graphite foils inserted between the die, punches and ceramic powder. It is known that some Ti^{4+} is reduced to Ti^{3+} during SPS sintering in argon atmosphere of ceramics based on $BaTiO_3$ [40]. Valdez-Nava et al. [40], proved by using electron probe microanalysis that the undoped and, La doped $BaTiO_3$ sintered by SPS are oxygen substoichiometry. The oxygen loss during the

Table 1 Rietveld refinement results on the $Ba_{1-x-y}Nd_xGa_yTiO_3$ pellets sintered by SPS, where x = 0.03–0.10 and y = 0.03

Samples $Ba_{1-x-y}Nd_xGa_yTiO_3$, y = 0.03 *x*	Lattice parameters (Å) *a*	Crystallite size (nm)	Volume (Å^3)
0.03	3.99775	114.16	63.892
0.05	3.99749	104.38	63.879
0.07	3.99639	69.94	63.827
0.10	3.99620	36.66	63.818

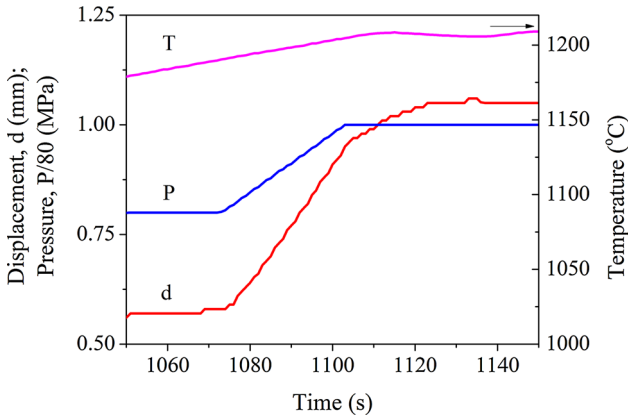

Fig. 1 Displacement (shrinkage—d), pressure (P) and sample temperature (T) versus time for the $Ba_{1-x-y}Nd_xGa_yTiO_3$ powder, with x = 0.1 and y = 0.03

sintering process varies with the temperature, the lanthanum content, the heating and cooling rate, the microstructure and the pellet density. The oxygen deficiency creates disequilibrium of the charge in the ceramics. It can be compensated by the electronic La donor doping effect where $Ba^{2+} = La^{3+} + e^-$ and the subsequent formation of Ti^{3+}; Ti^{3+} concentration increases with La-doping [40]. As example, they found Ti^{3+}/Ti^{4+} ratio 0.015 in $BaTiO_{3-x}$ and 0.036 in $Ba_{0.95}La_{0.05}TiO_{3-x}$. The reduced $BaTiO_{3-x}$ and $Ba_{0.95}La_{0.05}TiO_{3-x}$ are re-oxidized by annealing at 900 °C in air/oxygen after the SPS process. An optimal ratio temperature/time of annealing of SPS sintered pellets can lead to a complete removal of carbon derived from graphite die and oxygen vacancies from the dense pellets.

Our SPS sintered samples were annealed at 900 °C for 5 h in air, in order to restore the oxygen and Ti^{4+} stoichiometry and, to remove the carbon contamination.

The structure of the $Ba_{1-x-y}Nd_xGa_yTiO_3$ powders and sintered ceramics was investigated by X-ray diffraction (XRD) using a Bruker-AXS tip D8 ADVANCE diffractometer. CuK_α radiation (wavelength 1.5406 Å), LiF crystal monochromator and Bragg–Brentano diffraction geometry were employed. XRD data were acquired at 25 °C with a step-scan interval of 0.02° and a step time of 10 s. The microstructure of $Ba_{1-x-y}Nd_xGa_yTiO_3$ powders and SPS sintered pellets was examined using a FEI Quanta Inspect F SEM-EDAX scanning electron microscope.

Dielectric measurements were carried out in the metal-ferroelectric-metal (MFM) configuration, where M is silver and F is the $Ba_{1-x-y}Nd_xGa_yTiO_3$ pellets. Silver electrodes were screen-printed on both surfaces of the $Ba_{1-x-y}Nd_xGa_yTiO_3$ pellets. The frequency dependence of the dielectric constant (ε) and dielectric loss ($\tan\delta$) of the materials was obtained from electrical impedance values measured using an HIOKI 35 32-50 LCR Hi Tester.

Photoluminescence (PL), excitation spectra and PL lifetimes measurements were recorded at room temperature using a Jobin–Yvon Fluorolog spectrophotometer; the spectra were corrected for the spectral sensitivity.

3 Results

3.1 X-ray diffraction

The XRD patterns of $Ba_{1-x-y}Nd_xGa_yTiO_3$ gel calcined at 1100 °C, 3 h in air and of sintered pellets by SPS are shown in Figs. 2 and 3, respectively.

All the diffraction peaks of $Ba_{1-x-y}Nd_xGa_yTiO_3$ powders and sintered pellets are assigned to the cubic $BaTiO_3$ phase, *Pm–3m* space group and 221 space group number (Pattern: 16-6601, [41]).

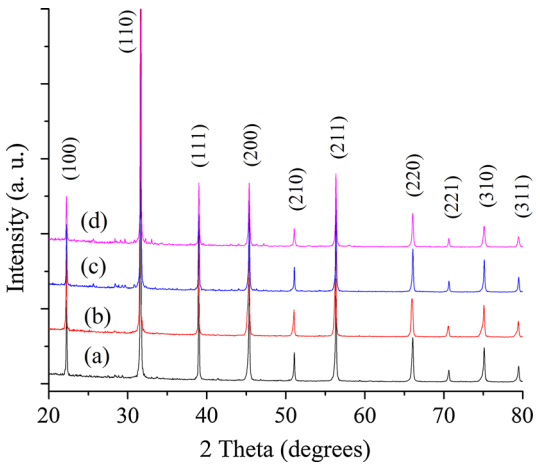

Fig. 2 XRD patterns (CuK_α radiation) of $Ba_{1-x-y}Nd_xGa_yTiO_3$, x = 0.03 (*a*), 0.05 (*b*), 0.07 (*c*) and 0.10 (*d*) precursor gels calcined at 1100 °C, 3 h

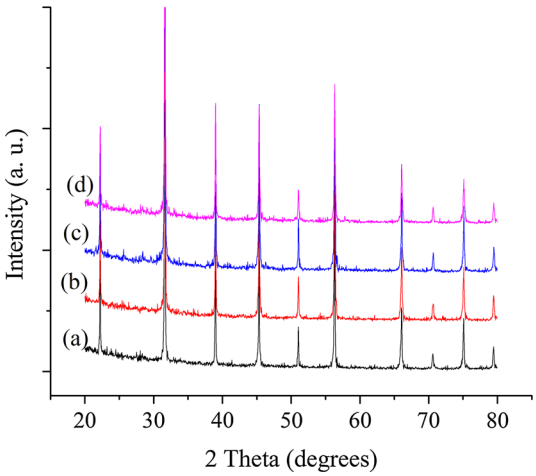

Fig. 3 XRD patterns of $Ba_{1-x-y}Nd_xGa_yTiO_3$ sintered pellets by SPS (2), where y = 0.03 for all samples, and *a* x = 0.03, *b* x = 0.05, *c* x = 0.07 and *d* x = 0.10, respectively

The diffraction data and patterns of $Ba_{1-x-y}Nd_xGa_yTiO_3$ ceramics (Fig. 3) were used to calculate the crystallographic characteristics of $Ba_{1-x-y}Nd_xGa_yTiO_3$ sintered ceramics. The unit cell parameters, crystallite size and volume of $Ba_{1-x-y}Nd_xGa_yTiO_3$ sintered pellets by SPS were calculated using Rietveld method [42] throughout the spectrum acquired in the program HighScore Plus 3.0e and are listed in Table 1.

Table 1 reveals that doping of $Ba_{0.97}Ga_{0.03}TiO_3$ with various amount of Nd (having ionic radius (r^{3+}_{Nd} = 1.26 Å) smaller than Ba (r^{3+}_{Ba} = 1.74 Å) reduce unit cell parameter, crystallite size and unit cell volume.

3.2 Microstructure

The morphology of $Ba_{1-x-y}Nd_xGa_yTiO_3$ powders and ceramics sintered by SPS method was investigated by electron microscopy, and the corresponding SEM images are presented in Figs. 4 and 5, respectively.

As can be seen in Fig. 4, the $Ba_{1-x-y}Nd_xGa_yTiO_3$ powders exhibit a high degree of coalescence. Some grains have a rounded shape and are connected through liquid phase. This type of microstructure with grains interconnected by liquid phase, is due to the high calcination temperature of $Ba_{1-x-y}Nd_xGa_yTiO_3$ powders (1100 °C),

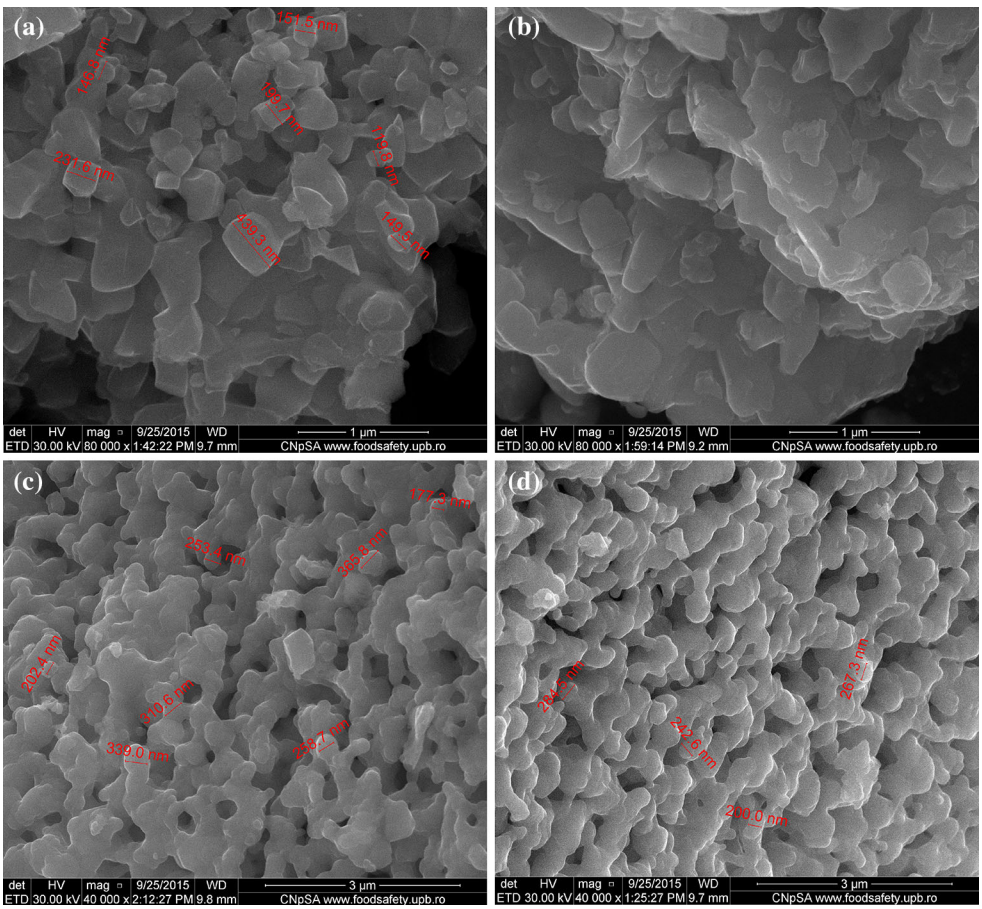

Fig. 4 SEM micrographs of the $Ba_{1-x-y}Nd_xGa_yTiO_3$ powders gel calcined at 1100 °C, 3 h in air; **a** x = 0.03, **b** x = 0.05, **c** x = 0.07 and **d** x = 0.10; y = 0.03

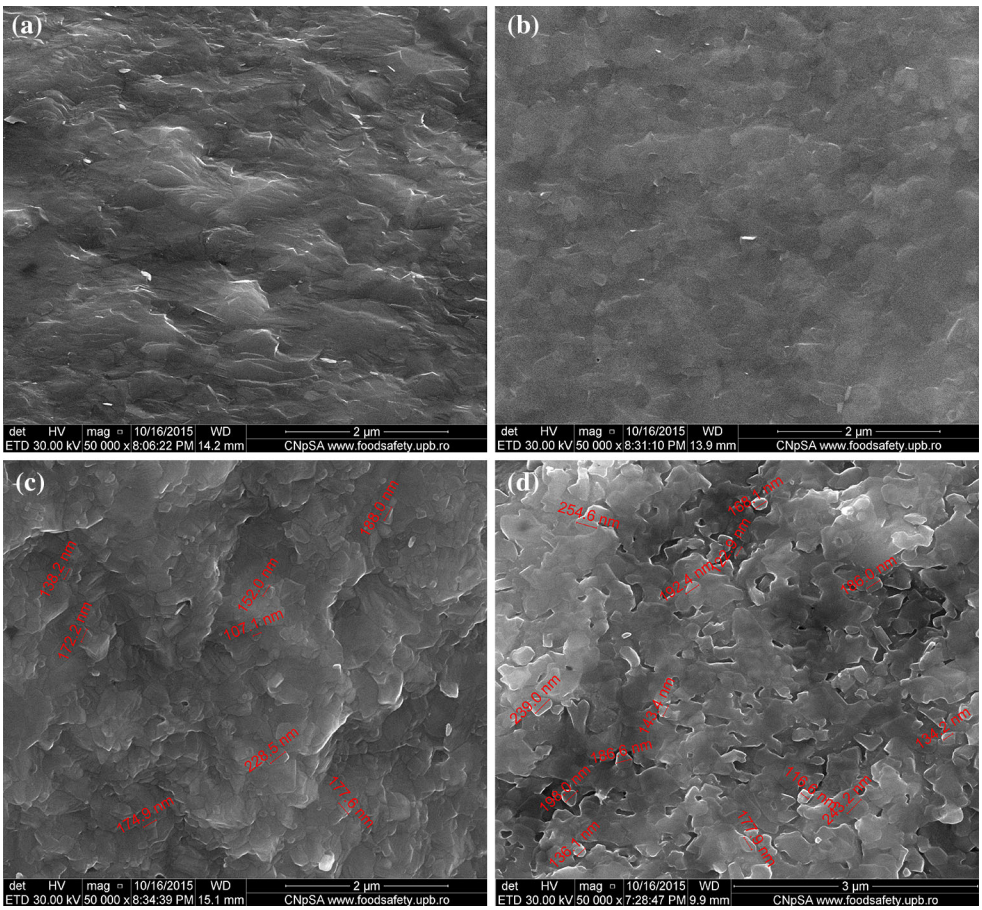

Fig. 5 SEM images of the $Ba_{1-x-y}Nd_xGa_yTiO_3$ sintered pellets by SPS; **a** x = 0.03, **b** x = 0.05, **c** x = 0.07 and **d** x = 0.10; y = 0.03

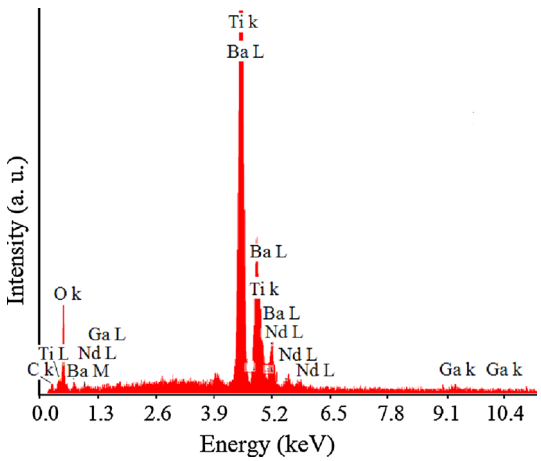

Fig. 6 Typical EDX spectra of $Ba_{1-x-y}Nd_xGa_yTiO_3$, x = 0.05 sintered pellet by SPS

required to obtain monophased powders. The average grain size decreases with increasing Nd concentration and it is between 300 and 200 nm (Fig. 4a–d).

The morphology of $Ba_{1-x-y}Nd_xGa_yTiO_3$ sintered pellets, observed by the SEM images presented in Fig. 5, is characteristic to the sintered ceramics by SPS, namely the liquid phase is present in large amounts and fills the pores between grains. Thus, the porosity of the samples almost disappears and densification is high. $Ba_{1-x-y}Nd_xGa_yTiO_3$ sintered samples show high apparent densities, which decrease with increasing Nd concentration (Table 1). Apparent densities of the sintered pellets were measured by Archimedes method (in toluene) using a density balance. The theoretical density of $BaTiO_3$ was considered 6.00 g/cm^3.

The chemical composition of the sintered pellets was analyzed using energy-dispersive X-ray spectroscopy (EDS) technique. A typical EDX spectra of $Ba_{1-x-y}Nd_xGa_yTiO_3$, x = 0.05 sintered pellet by SPS is shown in Fig. 6.

EDS analysis of the $Ba_{1-x-y}Nd_xGa_yTiO_3$, x = 0.05 and y = 0.03 sintered pellet confirms the presence of Ba, Nd, Ga, Ti, O and C elements. Very small amount of residual carbon can be observed on EDS spectra.

3.3 Dielectric characterization

$Ba_{1-x-y}Nd_xGa_yTiO_3$ ceramics sintered by SPS, with x = 0.03-0.10 and y = 0.03, were characterized in terms

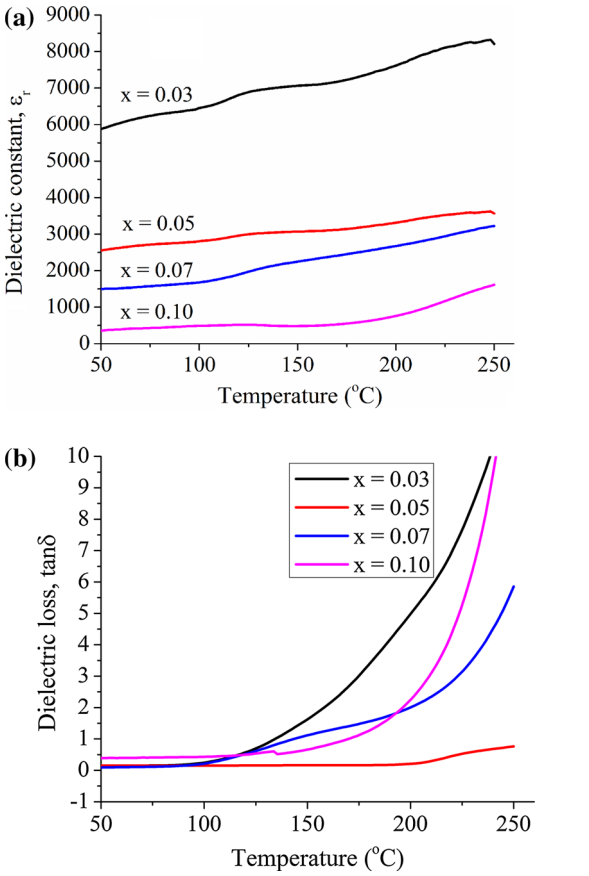

Fig. 7 Temperature dependence of the permittivity (**a**) and dielectric loss (**b**) measured at 1 kHz for $Ba_{1-x-y}Nd_xGa_yTiO_3$ pellets sintered by SPS, where x = 0.03–0.10 and y = 0.03

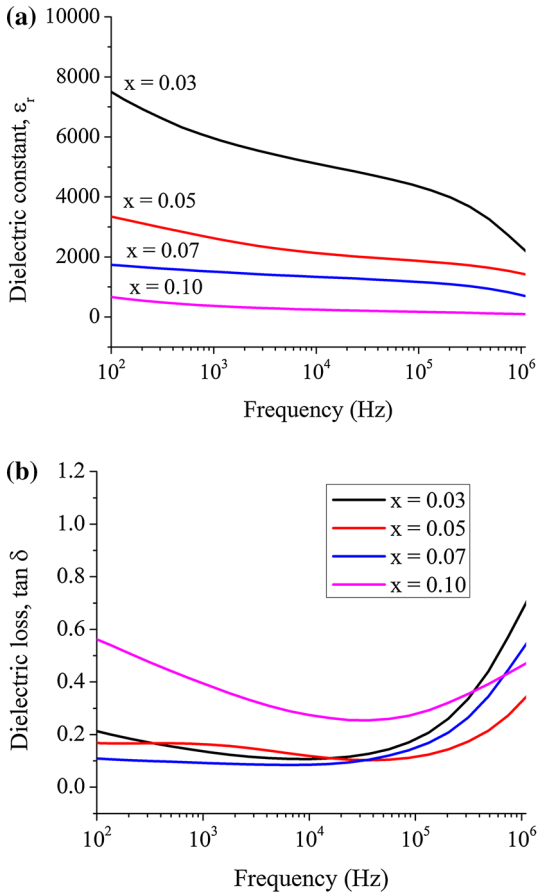

Fig. 8 Frequency dependence of dielectric constant (**a**) and dielectric loss (**b**) measured at 50 °C for $Ba_{1-x-y}Nd_xGa_yTiO_3$ pellets sintered by SPS, where x = 0.03–0.10 and y = 0.03

of temperature and frequency dependence of the permittivity and dielectric loss; the obtained results are presented in Figs. 6 and 7, and Table 2.

Concerning the Fig. 6a, the ε_r vs. temperature curves of $Ba_{1-x-y}Nd_xGa_yTiO_3$ samples exhibit broad dielectric peaks with a maximum at Curie temperature point (centred at $T_c \sim 125$ °C), especially visible for x = 0.03. A similar behavior was also observed by Gulwade et al. [43] which shown that La doped $BaTiO_3$ on the Ba site materials exhibits diffuse phase transition. These results indicate that the as-prepared $Ba_{1-x-y}Nd_xGa_yTiO_3$ ceramics are relaxors ferroelectric [44]. The specific structure of the sintered ceramics by spark plasma technique, characterized by high densification (as shown in Fig. 5), is responsible for the high value of dielectric constant and moderate dissipation factors (tan δ). The dielectric losses of $Ba_{1-x-y}Nd_xGa_yTiO_3$ ceramics increase drastically with temperature above ~150 °C, especially at low concentrations of Nd, due to the thermal conduction contribution.

The dielectric constant showed a high dissipation with frequency for small Nd concentrations (x = 0.03 and 0.05)

Table 2 Characteristics of $Ba_{1-x-y}Nd_xGa_yTiO_3$ ceramics sintered by SPS

Concentration x (at.%)	Sintering temperature (°C)	Sintering time (min)	Density ρ (g/cm$_3$)	Relative density ρ/ρ_{BaTiO3} (%)	Permitivity ε_r, at 1 kHz	Tan δ, at 1 kHz
0.03	1230	3	5.905	98.42	5890	0.13
0.05	1220	3	5.898	98.30	2560	0.15
0.07	1210	3	5.892	98.20	1500	0.09
0.10	1200	3	5.884	98.06	360	0.38

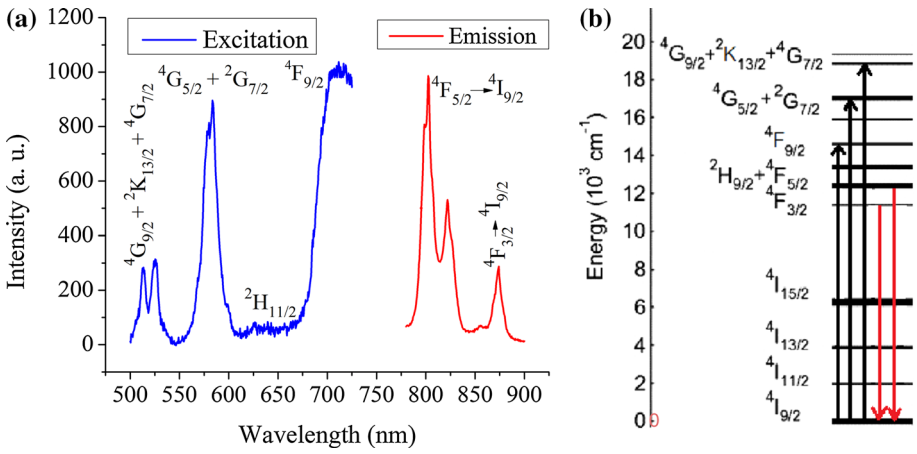

Fig. 9 **a** Normalized excitation spectrum of 800 nm luminescence and the photoluminescence spectrum excited at 580 nm recorded on $Ba_{1-x-y}Nd_xGa_yTiO_3$ samples, and **b** energy levels scheme of the Nd^{3+}-ions and the *f–f* transitions depicting the luminescence mechanisms

and decreases with increasing the amount of Nd (x = 0.07 and 0.10) added. The dielectric losses decrease at low-frequency and then increase as the frequency increased above 10^5 Hz (Fig. 7b), which can be ascribed to ionic conductivity. With increase of frequency, the decrease of polarization caused by ionic conductivity occurs, leading to increase of tan δ.

Dielectric losses of $Ba_{1-x-y}Nd_xGa_yTiO_3$ ceramics not vary linearly with the concentration of Nd, at room temperature and on the entire frequency interval 10^2–10^6 Hz. Variation of dielectric losses can be correlated with the structural inhomogeneities due to oxygen vacancies (VÖ) resulted from the sintering by SPS and barium vacancies (V_{Ba}'') caused by the substitution of Ba^{2+} with Nd^{3+} and Ga^{3+}.

We have not found any other study on $Ba_{1-x-y}Nd_xGa_yTiO_3$ ceramics. Therefore, it is not possible to compare our results on Nd, Ga codoped-$BaTiO_3$ materials with others, either electrically or photoluminescence. However, there are some papers on dielectric properties of $BaTiO_3$ doped with Ga or Ga, Y and Zn [28], and Nd doped-$BaTiO_3$ [19]. Compared with these reports, our $Ba_{1-x-y}Nd_xGa_yTiO_3$ ceramics sintered by SPS show improved dielectric properties.

3.4 Photoluminescence

Photoluminescence and excitation spectra, as well as the energy levels scheme of the Nd^{3+}-ions and the *f–f* transitions depicting the luminescence mechanisms of our $Ba_{1-x-y}Nd_xGa_yTiO_3$ powders calcined at 1100 °C, 3 h in air, are presented in Fig. 8. The recorded spectra are essentially the same, except the decrease of the luminescence intensity with the Nd^{3+} concentration.

Photoluminescence and excitation spectra of the Nd doped samples depicted in the Fig. 8 consist of characteristic bands ascribed to the f–f transitions. According to the Nd^{3+} energy levels scheme [45], the excitation spectrum is due to the transition between the ground $^4I_{9/2}$ state and various excited states, whereas the emission spectrum is due to the transitions from the $^4F_{3/2}$, and ($^2H_{9/2}$ + $^4F_{5/2}$) levels (Fig. 8a). The time decay profiles of the red emission band (at 800 nm) recorded under 580 nm excitation (not shown here) are in the sub-milliseconds range. The profiles are single exponential decay curves. The characteristic lifetimes appear to decrease with increasing the Nd^{3+} concentration in the matrix, as follows: 0.182 ± 0.03 ms (x = 0.03), 0.155 ± 0.03 ms (x = 0.05), 0.110 ± 0.03 ms (x = 0.07) and 0.101 ± 0.03 ms (x = 0.1) (Fig. 9).

The emission intensity decreases along with decrease of decay time and increasing of Nd doping and, can be interpreted as a concentration dependent enhancement of non-radiative de-excitation processes caused by cross-relaxation process between neighboring Nd^{3+} ions [46].

4 Conclusions

$Ba_{1-x-y}Nd_xGa_yTiO_3$ powders and ceramics, with x varying from 0.03 to 0.10, and y = 0.03 were successfully prepared using the sol–gel method and SPS technique. In order to prepare monophased powders of $Ba_{1-x-y}Nd_xGa_yTiO_3$, the gel powders were calcined at 1100 °C and grains of 200–300 nm size were obtained. Solid solutions of the type $Ba_{1-x-y}Nd_xGa_yTiO_3$ ceramics sintered by SPS exhibited a diffuse transition as well as a deviation from Curie–Weiss law, a high dielectric constant and low loss. Increases of neodymium content lead to lower values of crystallographic characteristics of barium titanate substituted with 3 at.% Ga. The luminescence spectra recorded on the powders have shown hot Nd-ion emission (at 800 nm) from the 4F5/2 level and concentration quenching effects. These materials ($Ba_{1-x-y}Nd_xGa_yTiO_3$) have potential applications in optical devices and ceramic capacitors. Also, this work may lead to

the development of a novel material as a result of simultaneous doping of Nd and Ga.

Acknowledgments Author Catalina Andreea Vasilescu gratefully acknowledges the financial support from the Sectorial Operational Programme Human Resources Development 2007–2013 of the Ministry of European Funds through the Financial Agreement POSDRU/159/1.5/S/132397 (ExcelDOC).

References

1. D. Staedler, T. Magouroux, H. Rachid, C. Joulaud, J. Extermann, S. Schwung, S. Passemard, C. Kasparian, G. Clarke, M. Gerrmann et al., ACS Nano **6**, 2542–2549 (2012)
2. C.M. Krowne, S.W. Kirchoefer, W. Chang, J.M. Pond, L.M.B. Alldredge, Nano Lett. **11**, 988–992 (2011)
3. S.B. Qin, D. Liu, Z.Y. Zuo, Y.H. Sang, X.L. Zhang, F.F. Zheng, H. Liu, X.G. Xu, J. Phys. Chem. Lett. **1**, 238–241 (2010)
4. C.Y. Fang, C.A. Randal, M.T. Lanagan, D.K. Agrawal, J. Electroceram. **22**, 125–130 (2009)
5. V. Swaminathan, S.S. Pramana, T.J. White, L. Chen, R. Chukka, Appl. Mater. Interf. **2**, 3037–3042 (2010)
6. L. Huang, Z. Chen, J. Wilson, S. Banerjee, R.D. Robinson, I.P. Herman, R. Laibowitz, S. O'Brien, J. Appl. Phys. **100**, 034316 (2006)
7. T. Takagahara, K. Takeda, Phys. Rev. B **46**, 15578–15581 (1992)
8. J. Yu, J. Sun, J. Chu, D. Tang, Appl. Phys. Lett. **77**, 2807–2810 (2000)
9. A. Mazur, O.F. Schirmer, S. Mendricks, Appl. Phys. Lett. **70**, 2395–2397 (1997)
10. P. Barik, T.K. Kundu, Nanosyst. Phys Chem. Math. **4**, 269–275 (2013)
11. Z. Fu, B.K. Moon, H.K. Yang, J.H. Jeong, J. Phys. Chem. C **112**, 5724–5728 (2008)
12. R. Pazik, R.J. Wiglusz, W. Strek, Mater. Res. Bull. **44**, 1328–1333 (2009)
13. G.C. Yi, B.A. Block, G.M. Ford, B.W. Wessels, Appl. Phys. Lett. **73**, 1625–1627 (1998)
14. M.A. Garcia, R.F.J. Carrillo, H.M. Garcia, G.O. Barbosa, N.A. Meneses, S.S. Palomares, V.A. Flores, Mater. Trans. **50**, 1850–1854 (2009)
15. P.M.M. Vijatovic, J.D. Bobic, T. Ramoska, J. Banys, B.D. Stojanovic, Mater. Charact. **62**, 1000–1006 (2011)
16. N. Maso, H. Beltran, E. Cordoncillo, F.A. Arenas, P. Escribano, D.C. Sinclair, A.R. West, J. Mater. Chem. **16**, 3114–3119 (2006)
17. B. Sarkar, K. Chakrabarti, K. Das, S.K. De, Phys. D: Appl. Phys. **45**, 505304–505313 (2012)
18. L. Ben, D.C. Sinclair, Appl. Phys. Lett. **98**, 092907 (2011)
19. Z. Yao, H. Liu, Y. Liu, Z. Wu, Z. Shen, Y. Liu, M. Cao, Mater. Chem. Phys. **109**, 475–481 (2008)
20. Y. Li, X. Yao, L. Zhang, Ceram. Int. **30**, 1325–1328 (2004)
21. T. Hashishin, E. Sato, S. Umeki, K. Kojima, J. Tamaki, Mater. Sci. Eng. **18**, 092031 (2011)
22. R. Pazik, D. Hreniak, W. Strek, Mater. Sci-Poland **22**, 219–225 (2004)
23. W. Zhang, L. Cao, W. Wang, G. Su, W. Liu, Ceram-Silikaty **57**, 146–150 (2013)
24. J.L. Jou, C.M. Lei, Y.W. Xu, W.C.V. Yeh, Chin. J. Phys. **50**, 926–931 (2012)
25. M.J. Wang, H. Yang, Q.L. Zhang, Z.S. Lin, Z.S. Zhang, D. Yu, L. Hu, Mater. Res. Bull. **60**, 485–491 (2014)
26. D. Gulwade, P. Gopalan, Physica B **404**, 1799–1805 (2009)
27. H. Natsui, C. Moriyoshi, F. Yoshida, Y. Kuroiwa, T. Ishii, O. Odawara, J. Yu, S. Yoda, Appl. Phys. Lett. **98**, 132909–132911 (2011)
28. M.J. Wang, H. Yang, Q.L. Zhang, L. Hu, D. Yu, Z.S. Lin, Z.S. Zhang, J. Mater. Sci.: Mater. Electron. **25**, 2905–2912 (2014)
29. Q. Zhou, C.R. Zhou, H.B. Yang, C.L. Yuan, G.H. Chen, L. Cao, Q.L. Fan, J. Mater. Sci.: Mater. Electron. **25**, 196–201 (2014)
30. S.Y. Kang, Y.H. Kim, J. Moon, K.S. Suh, D.J. Lee, S.G. Kang, Jpn. J. Appl. Phys. **48**, 052301 (2009)
31. K. Sadhana, T. Krishnaveni, K. Praveena, S. Bharadwaj, S.R. Murthy, Scripta Mater. **59**, 495–498 (2008)
32. P. Kuruva, U.M.S. Rajaputra, S. Sanyadanam, R.M. Sarabu, Turk. J. Phys. **37**, 312–321 (2013)
33. H. Maiwa, Jpn. J. Appl. Phys. **47**, 7646–7649 (2008)
34. Z. Chen, F. Zhou, M. Liu, G. Wu, X. Pan, Ferroelectrics **123**, 61–67 (1991)
35. W. Luan, L. Gao, H. Kawaoka, T. Sekino, K. Niihara, Ceram. Int. **30**, 405–410 (2004)
36. M.S. Spotz, D.J. Skamser, D.L. Johnson, J. Am. Ceram. Soc. **78**, 1041–1048 (1995)
37. D. Clark, W.H. Sutton, Annu. Rev. Mater. Sci. **26**, 299–331 (1996)
38. D.K. Agrawal, Solid State Mat. Sci. **3**, 480–486 (1998)
39. J.G.P. Binner, B. Vaidhyanathan, Key Eng. Mat. **264–268**, 725–730 (2004)
40. Z. Valdez-Nava, S. Guillemet-Fritsch, C. Tenailleau, T. Lebey, B. Durand, J.Y. Chane-Ching, J. Electroceram. **22**, 238–244 (2009)
41. V.I. Petkov, V. Buscaglia, M.T. Buscaglia, Z. Zhao, Y. Ren, Phys. Rev. B: Condens. Matter. Mater. Phys. **78**, 054107 (2008)
42. H.M. Rietveld, J. Appl. Crystallogr. **2**, 65–71 (1969)
43. D. Gulwade, P. Gopalan, Phys. B **404**, 1799–1805 (2009)
44. N. Thomas, J. Phys. Chem. Solids **51**, 1419 (1990)
45. W.T. Carnall, G.L. Goodman, K. Rajnak, R.S. Rana, J. Chem. Phys. **90**, 3443–3457 (1989)
46. A. Bednarkiewicz, D. Wawrzynczyk, M. Nyk, W. Strek, Opt. Mater. **33**, 1481–1486 (2011)